Applied Catalysis A, General 623 (2021) 118292

Contents lists available at ScienceDirect

Applied Catalysis A, General

journal homepage: www.elsevier.com/locate/apcata

Molybdate Stabilized Magnesium-Iron Hydrotalcite Materials: Potential Catalysts for Isoeugenol to Vanillin and Olefin Epoxidation

P.P. Neethu, A. Sreenavya, A. Sakthivel *

Inorganic Materials & Heterogeneous Catalysis Laboratory, Department of Chemistry, School of Physical Sciences, Central University of Kerala, Kasaragod, Kerala, 671320, India

ARTICLE INFO

Keywords:
Molybdenum
Vanillin
Iron
Oxidation
Olefin
Iso-eugenol
Hydrotalcite

ABSTRACT

A series of molybdate-intercalated and stabilized magnesium-iron hydrotalcite (HMFeMo) materials with different molybdate loadings were successfully prepared by an in-*situ* hydrothermal method. The prepared HMFeMo materials were systematically characterized using Fourier-transform infrared spectroscopy (FT-IR), powder X-ray diffraction (XRD), Ultraviolet-visible spectroscopy, scanning electron microscopy, thermo-gravimetric analysis, nitrogen adsorption-desorption and X-ray photoelectron spectroscopy (XPS) experiments. The XRD results demonstrated the successful intercalation of molybdate ions in the interlayer space of magnesium-iron hydrotalcite and the stabilization of the layered structure. In addition, the XPS spectra of the HMFeMo materials revealed the presence of molybdenum in a higher-valent oxidation state. The calcination of HMFeMo materials led to the formation of solid solution of mixed metal oxides. Both the as-prepared and calcined HMFeMo catalysts showed promising activity for the epoxidation of cyclooctene, as a model reaction. Furthermore, the performance of the as-prepared and calcined HMFeMo catalysts for the oxidation of a biomass model compound, namely isoeugenol to vanillin, was evaluated. The isoeugenol conversion over the as-prepared HMFeMo catalysts under solvent-free conditions and using *tertiary*-butyl hydroperoxide in decane as the oxidant was good. Moreover, the isoeugenol conversion and selectivity toward vanillin of HMFeMo0.1, with a molybdate loading of 0.1 mol %, were the highest (86.2% and 83.1%, respectively) of all HMFeMo catalysts in this study at 80 °C for 5 hr. HMFeMo0.1 presented the best catalytic activity for both the epoxidation of cyclooctene and oxidation of isoeugenol to vanillin, and its activity remained unchanged after several runs.

1. Introduction

Hydrotalcite (HT) materials are well known as potential catalyst precursors and supports for several organic reactions [1]. Compared with bulk oxides as support materials, HT materials present attractive properties, such as a good anion exchange capacity, tunable acid base and redox properties, remarkable activity, low waste formation, and facile product recovery [2]. The general formula of HTs is $[M(II)_{(1-x)}M(III)_x(OH)_2]^{x+}[A^{n-}_{x/n}]\cdot mH_2O$, where M(II) and M(III) are divalent and trivalent metals, respectively, and A is an interlayer anion [3,4] and tailor-made HT-based catalysts with different compositions, viz., cations in the brucite layer, and anions in the interlayer region can be fabricated. Iron-based catalysts have invariably contributed to mankind's progress owing to their involvement in the Haber-Bosch and Fischer--Tropsch processes. Iron-based catalysts can be used for several organic transformations [5] and, particularly, magnesium–iron HTs are used for Friedel-Crafts alkylation [6,7], Baeyer-Villiger oxidation [8], and aromatic nitro compound reactions [9].

Stabilization of the interlayer spaces of HTs using anions, such as silicate, molybdate, vanadate and phosphate enhance the number of exposed active sites and improves the catalytic activity of HTs [1, 10-14]. Furthermore, the chemical, magnetic, electronic, and optical properties of the host HT can be tuned using different intercalated anions [1]. The intercalation of different poly-oxometallates facilitated the development of catalysts with attractive acid bases and redox properties [10–14]. Poly-oxometallate-intercalated layered double hydroxides have been used for epoxidation, esterification, photo-degradation, per-oxidation, and alkoxylation reactions [10–12].

To date, the limited studies are known on catalytic activity of molybdate-intercalated HT materials for organic processes, such as propane dehydrogenation [13], *tertiary* butanethiol oxidation [14], and styrene oxidation with air [15]. The typical oxidation state of

* Corresponding author.
E-mail address: sakthiveldu@gmail.com (A. Sakthivel).

https://doi.org/10.1016/j.apcata.2021.118292
Received 7 April 2021; Received in revised form 12 July 2021; Accepted 17 July 2021
Available online 21 July 2021

molybdenum varies from -2 to +6, and the coordination number of molybdenum ranges from 4 to 6; moreover, molybdenum species present different stereo-chemistries, and can form bi- and poly-nuclear compounds with many organic and inorganic ligands. Owing to the aforementioned properties, molybdenum can be used to develop new catalysts with attractive potential applications. Molybdenum-containing catalysts are widely used for organic reactions, such as epoxidation, metathesis, hydroformylation, and C–H activation [16,17]. Several cyclopentadienyl molybdenum complexes have been used for various oxidation reactions. Researchers have grafted molybdenum complexes on supports, such as MCM-41, MCM-48, and SBA-15, and the catalytic activity of molybdenum toward oxidation reactions has been well established [17]. However, to date, the introduction of molybdate ions into HT materials and evaluation of their catalytic activity has been limited. Molybdenum–iron centers are known as potential nitrogen-fixation cofactors in biological systems. Therefore, the development of molybdenum–iron-based HT materials and exploration of their redox properties for oxidation of biomass-derived model components are attractive research topics. Among biomass-derived model components, isoeugenol has received increasing attention because the selective oxidation of isoeugenol to vanillin is an important process in the fine chemical industry.

Vanillin, which is an important flavor and aroma compound, is present in vanilla and is mainly used in the food, cosmetic, perfume, and pharmaceutical industries [18]. Moreover, vanillin has been used to manufacture thermoplastics [19]. Vanillin is produced worldwide using different sources, such as oil (85%), biomass (15%), and orchid pods (<1%) [20]. Because vanillin natural resources are increasingly scarce, many cost-effective methods are used for the industrial production of vanillin. Recently, one of the primary methods for the production of vanillin from lignin-derived feed-stocks, such as isoeugenol, has attracted increasing attention, and several reports regarding the synthesis of vanillin from isoeugenol have been published. Isoeugenol was oxidized to vanillin using graphene oxide-supported copper oxide with a vanillin yield of 53% under mild reaction conditions [21]. Aluminosilicate-supported transition metal catalysts have also been used to produce vanillin. The conversion and selectivity for the oxidation of isoeugenol using H_2O_2 as a green oxidizing agent over niobium-incorporated catalysts yielded only 46 % vanillin [22]. Gusevskaya et al. reported the oxidation of isoeugenol to vanillin over a n-Bu_4NVO_3/pyrazine-2-carboxylic acid catalyst combination [23]. The typical vanillin synthesis method from eugenol involves two steps: eugenol isomerization to isoeugenol and isoeugenol oxidation to vanillin. In contrast, a direct one-step method was developed for the oxidation of eugenol to vanillin using a cobalt-based catalyst [24]. Among the various catalysts used for isoegenol oxidation the catalyst prepared by Shimazu et al. showed the highest conversion for isoeugenol. They synthesized a cobalt porphyrin intercalated into lithium taeniolite clay to oxidize isoeugenol using molecular oxygen as the oxidant and achieved a highest vanillin yield of 72 % [25]. But, the preparation of the catalyst involved complex synthetic procedure. Recently, cerium-containing zeolite, viz., MCM-22 and molybdenum incorporated MCM-22 are explored as catalysts for the oxidation of isoeugenol [26]. However, the selectivity towards vanillin always limited and the development of catalyst for selective oxidation of isoeugenol to vanillin is an important area of research in recent years. The present catalyst showed improved selectivity with good conversion of isoeugenol.

Therefore, designing a highly active, selective, and cost-effective catalyst for the conversion of isoeugenol to vanillin is of potential interest for researchers. In this study, we evaluated the structural properties and catalytic activity of magnesium–iron HT-like materials with molybdate anions in the interlayer region. Furthermore, the catalytic activity of molybdate-intercalated magnesium–iron HT-like materials for isoeugenol oxidation to vanillin was investigated. In addition, the activity of the synthesized catalysts for cyclooctene epoxidation was evaluated. To the best of our knowledge, this is the first report on the conversion of isoeugenol to vanillin over a HT-like material.

2. Experimental

2.1. Materials

Magnesium nitrate hexahydrate ($Mg(NO_3)_2{\cdot}6H_2O$ (Merck)), Ammonium heptamolybdate tetrahydrate ($(NH_4)_6Mo_7O_{24}{\cdot}4H_2O$ (SRL)), Ferric nitrate nonahydrate ($Fe(NO_3)_3{\cdot}9H_2O$ (LOBA)), aqueous ammonia solution (25 %; SRL) were used as starting material for synthesis. For carrying out the reaction, cyclooctene (Spectrochem), *tertiary*-Butyl hydroperoxide solution 5.0-6.0 M in decane (Sigma Aldrich), isopropyl alcohol (LOBA), isoeugenol (Avra), acetonitrile (Merck) were used.

2.2. Catalyst preparation

Molybdate-intercalated and stabilized magnesium–iron HT (HMFeMo) catalysts were prepared using an *in situ* hydrothermal method, as follows [4,27]. Solution 1 was prepared by adding $Mg(NO_3)_2{\cdot}6H_2O$ (45.54 mmol) and $Fe(NO_3)_3{\cdot}9H_2O$ (15 mmol) to deionized water (120 mL). Solution 2 was prepared by adding $(NH_4)_6Mo_7O_{24}{\cdot}4H_2O$ (4.54 mmol) and aqueous ammonia (NH_3aq.10 mL) to deionized water (100 mL). Solution 1 was added to solution 2 dropwise at 60 °C under vigorous stirring. Precipitation was observed at a final gel pH of 9.0. After precipitation was completed, the slurry was transferred to a stainless-steel autoclave and aged at 100 °C for 4 d. The precipitate was filtered and washed with deionized water until the pH of the filtrate reached 7, followed by drying at 80 °C. The catalysts with ammonium hepta-molybdate loadings of 0.02, 0.05, 0.1 and 0.15 mole with respect to 1 mole of magnesium in the gel are denoted as HMFeMo 0.02, HMFeMo 0.05, HMFeMo 0.1, and HMFeMo 0.15, respectively. For comparison, a carbonate intercalated magnesium–iron HT (HMFe) material was also prepared using the same procedure without molybdenum source. The synthesized HMFeMo catalysts were calcined at different temperatures (T), and the calcined samples are hereafter denoted as HMFeMoC-T, where T represent the calcination temperature.

2.3. Material characterization

The powder X-ray diffraction (XRD) patterns of the synthesized catalysts were recorded on a MiniFlex (300/600) (Rigaku, Japan) XRD instrument with Cu Kα radiation (λ =1.54059 Å) in the 2θ range of 3-80° at a scan speed of 0.05 and step size of 0.5°. The Fourier-transform infrared (FT-IR) spectra of the catalysts were obtained using a FT/IR-4700 (JASCO, Japan) spectrometer in the wavenumber range of 4000-400 cm^{-1}. The diffuse reflectance ultraviolet–visible (UV–vis) spectra of the catalysts were recorded (200–800 nm), by using a UV-visible spectrophotometer (UV2600 Shimadzu, Japan), and $BaSO_4$ as a reference. Thermo-gravimetric analysis (TGA) of the catalysts was performed using a STA 6000 (Perkin Elmer, Germany) simultaneous thermal analyzer. About 2–5 mg of the sample was taken in the silica crucible and heated under a nitrogen atmosphere with a heating rate of 10 °C/min, ranging from 40 to 900 °C. The scanning electron microscopy (SEM) images of the catalysts were obtained using a SEM (Phillips Technai G2 T30 SEM) operated at 300 Kv. The X-ray photoelectron spectroscopy (XPS) profiles of the samples were obtained using a photoelectron spectrometer (Prevac, Poland) that was equipped with a VG Scienta's R3000HP analyser and a MX650 monochromator. Nitrogen adsorption–desorption experiments were performed at −196 °C using an ASAP 2020 (Micromeritics USA) automatic micropore physisorption analyzer after the samples were degassed at 200℃ for at least 8 h under 10^{-3} Torr pressure prior to each run.

2.4. Cyclooctene oxidation

Catalytic oxidation of cyclooctene using *tertiary*-butyl hydroperoxide (TBHP) in decane as the oxidizing agent was performed in a 25 mL two-necked round-bottom flask. For a typical procedure, 2 mmol of cyclooctene and 0.025 g of catalyst were added to the flask and magnetically stirred at the desired reaction temperature. Thereafter, 2 mmol of TBHP in decane was added dropwise to the reaction mixture. After the reaction was completed, the products were extracted by adding 1 mL of isopropanol to the reaction mixture and were subsequently analyzed using agas chromatography (GC; Mayura Analytical GC 1100, India) instrument with a flame ionization detector connected with AB-Innowax column (30 m length and 0.25 mm internal diameter).

2.5. Isoeugenol oxidation

The isoeugenol oxidation reaction (Scheme 1) using TBHP in decane as the oxidizing agent was performed in a 25 mL round-bottom flask. Isoeugenol (2 mmol) and catalyst (0.05 g) were added to the flask and magnetically stirred at the desired reaction temperature. TBHP in decane was added dropwise to the reaction mixture. After the reaction was completed, the products were extracted by adding 4 mL acetonitrile to the reaction mixture and were subsequently analyzed using the aforementioned GC instrument.

3. Results and discussion

3.1. Catalyst characterization

The FT-IR spectra of the as-synthesized and calcined HMFeMo materials are illustrated in Fig. 1 and Fig. S1, respectively. The broad vibration band at approximately 3260 cm^{-1} corresponded to the stretching of hydrogen-bonded hydroxyl (–OH) groups of the surface-adsorbed and interlayer water molecules present in the HMFeMo materials. The bands at approximately 1635 cm^{-1} were ascribed to the bending vibrations of water molecules. The sharp bands at 1412 and 1484 cm^{-1} in the FT-IR spectrum of HMFe were attributed to the vibrational modes of the interlayer carbonate anions. The band at 913 cm^{-1} in the FT-IR spectra of the HMFeMo materials was characteristic of the vibrations of the Mo=O bonds of the interlayer molybdate ions in the catalyst. In addition, the band at approximately 845 cm^{-1} was characteristic of the Mo–O–Mo stretching vibrations of the molybdate ions in the interlayer region [10,15]. The absorption band at 1386 cm^{-1} in the FT-IR spectra of HMFeMo corresponded to the asymmetric stretch of carbonate ions, indicating that traces of carbonate ions were present in the interlayer region. The presence of a shoulder band at approximately 1386 cm^{-1} with increasing molybdate loading was attributed to the disordered nature of the interlayer region; however, it can also be ascribed to the decrease in symmetry of carbonate ions [28]. With increasing molybdate loading, the intensity of the band corresponding to –OH stretching decreased. This was attributed to the intercalation of molybdate anions in the interlayer region, which can lead to a decrease in the number of hydrogen bonds. The bands at 795 and 883 cm^{-1} in the FT-IR spectra of the HMFeMo samples corresponded to the OH bending

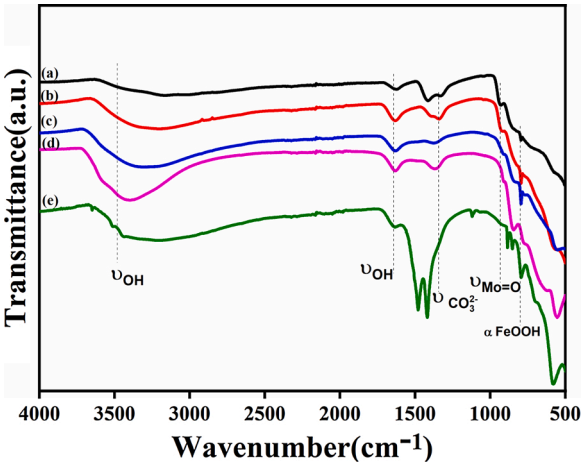

Fig. 1. Fourier-transform infrared spectra of as-prepared (a) HMFeMo0.15, (b) HMFeMo0.10, (c) HMFeMo0.05, (d) HMFeMo0.02, and (e) HMFe.

modes of α-FeOOH [29]. The vibrational bands at 973, 835, and 547 cm^{-1} in the FT-IR spectra of the calcined samples corresponded to terminal M = O stretching, antisymmetric Mo–O–Mo, and Fe_2O_3, respectively [30].

The powder XRD patterns of the as-synthesized HMFeMo samples are presented in Fig. 2 and confirmed the layered hydrotalcite structure of the synthesized materials. The broad peaks at 2θ value of 11.5°, 23.1°, 34.7°, 59.5°, and 61.2° in the XRD patterns of the as-synthesized HMFeMo samples corresponded to the (003), (006), (012), (110), and (113) planes, respectively, of layered hydrotalcite materials [15]. As molybdate loading increased, the aforementioned peaks broadened, confirming that molybdate ions were intercalated in the interlayer space

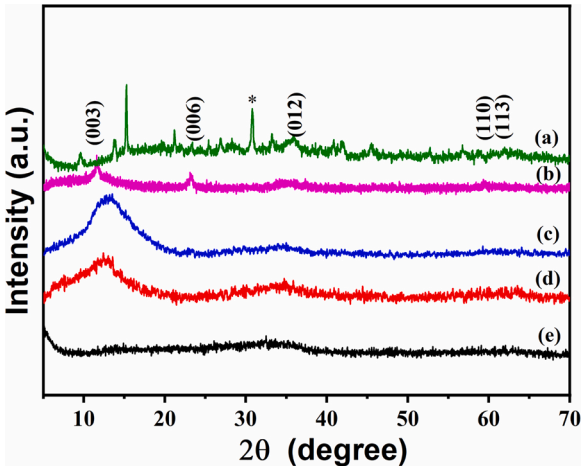

Fig. 2. Powder X-ray diffraction patterns of as-synthesized (a)HMFe, (b) HMFeMo0.02, (c) HMFeMo0.05, (d) HMFeMo0.10, and (e) HMFeMo0.15.

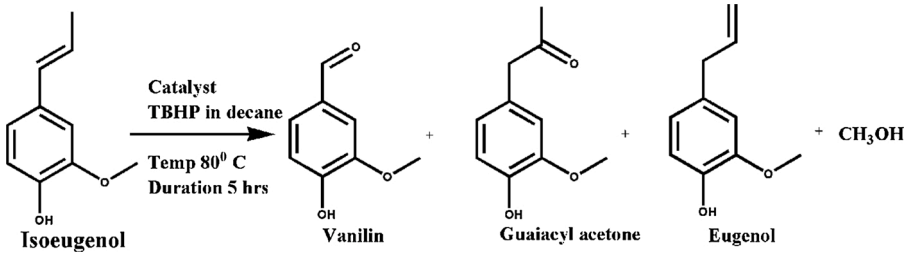

Scheme 1. Isoeugenol oxidation to vanillin over HMFeMo catalysts.

of the layered structures [4]. The peaks in the XRD pattern of HMFeMo0.15 with a high molybdate loading were very broad. The XRD pattern of pure HMFe revealed that HMFe presented a HT structure with minor (Fe_2O_3 orthorhombic) impurity phases. The XRD patterns of the HMFeMoC-T samples are presented in Fig. S2. The XRD patterns of the samples calcined at 800 °C included characteristic peaks of $MgFe_2O_4$ spinel (30.1°, 35.3°, 43.02°, 57.03°, and 62.4°) [31], Mo_2O_5 and Fe_2O_3 (hematite) phases.

The coordination and oxidation states of iron and molybdenum species present in the HMFe and HMFeMo samples were analyzed using DRUV–Visible spectroscopy, and the results are presented in Fig. 3. The HMFe material showed two distinguish absorption bands appeared around 220 nm and 305 nm, can be assigned as ligand to metal charge transfer bands of trivalent iron species present in the octahedral coordination of the layered hydrotalcite framework. Further an additional broad band above 450 nm is arising from the presence of bulk iron oxyhydroxy species present in the uniform layer of hydrotalcite framework of HMFe sample [32,33]. The introduction of molybdate ions in the interlayer of HMFe results overlapping of charge transfer peaks due to Fe^{3+} ions and showed broad absorption band in the wavelength region of 210-285 nm, which was assigned to the charge transfer from O^{2-} to Mo^{6+} ions in isolated molybdate (MoO_4^{2-}) species present in the interlayer space of hydrotalcite. As molybdate content increased (HMFeMo0.15), the absorption bands become much broader and shifts to higher wavelength, indicating the presence of octahedrally coordinated molybdenum polyoxoanions[15,34] present on the interlayer space.

The SEM images of the HMFeMo catalysts (Fig. 4) were used to analyze catalyst morphology. The as-prepared HMFe sample presented a semi-crystalline morphology. The molybdate-intercalated HMFeMo0.1 catalyst consisted of ordered particles with sizes in the micrometer range. The HMFeMoC0.1-800 sample comprised tiny particles with a uniform spherical morphology, indicating that particle size decreased upon calcination. The calcined HMFe sample presented a flower-like morphology.

The behavior of HMFe and HMFeMo0.1 during thermal decomposition was analyzed using TGA, and the TGA curves are presented in Fig. 5. The thermal behavior of the HMFe and HMFeMo 0.1 samples was showed different thermal decomposition behavior. The HMFe sample exhibited three major weight loss stages. The first weight loss stage (<130 °C) corresponded to the removal of physically adsorbed water. The second weight loss stage (130-370 °C) was attributed to the removal of chemically adsorbed water present in the internal and external surfaces of HT. The last decomposition stage (370-450 °C) corresponded to the removal of interlayer carbonate anions and dehydroxylation of intralayer hydroxyl groups. The total weight loss of HMFe was 28 %. The HMFeMo0.1 sample presented a single-stage decomposition with a maximum weight loss of 18 %. The smaller weight loss of the HMFeMo0.1 sample indicated that molybdenum intercalation increased thermal stability [4,14,35].

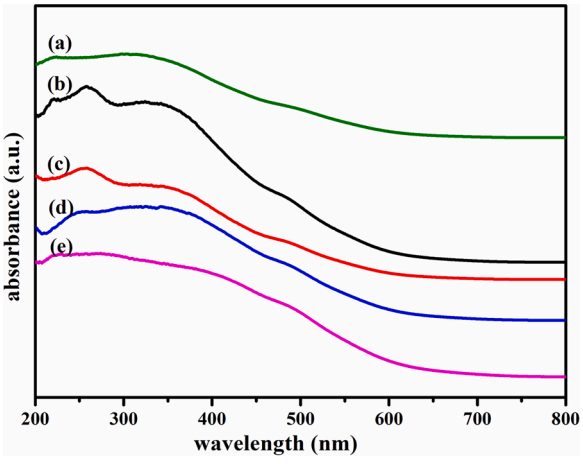

Fig. 3. Diffuse reflectance ultraviolet–visible spectra of as-synthesized (a) HMFe (b) HMFeMo0.02, (c)HMFeMo0.05, (d)HMFeMo0.10, and (e)HMFeMo0.15.

The nitrogen adsorption–desorption isotherms of the HMFe and HMFeMo samples are illustrated in Fig. 6. The HMFe and HMFeMo0.05 (Fig. 6 (d) and (c) respectively) materials showed continuous adsorption with distinct H3 type hysteresis loops at p/p_0 range of 0.8 to 0.9, characteristic of layered hydrotalcite with inter-particles mesoporous structure [36]. The surface areas and pore volumes of the samples are summarized in Table 1. The BET surface area of HMFe and HMFeMo0.05 were found to be 77 m^2/g. The surface area of the more molybdate intercalated HT samples (HMFeMo0.1and HMFeMo0.15) is higher than those of the HMFe and HMFeMo0.05 samples. The increase in concentration of molybdate anions (HMFeMo0.1 and HMFeMo0.15) in the synthesis gel facilitate uniform condensation of molybdate ions in the interlayer domain of layered HT structure and results an increase in surface area and micropore volume as evident from sharp uptake in the p/p_0 range of below 0.1. The behavior is analogues to the hard-silicate anion intercalation on HT layer [4] and making the interlayer surface more accessible [4,37]. A slight decrease in the surface area (177 m^2/g) for the HMFeMo0.15sample was a result of the filling of the pore surfaces and HT interlayer by molybdenum polyoxoanions. The decrease in surface area of the calcined sample (HMFeMoC0.1-800) was attributed to the formation of crystalline bulk metal oxide [38,4].

The oxidation state of the iron and molybdenum species present on the surface of the HMFeMoC0.1-800 sample was analyzed using XPS, and the deconvoluted results are presented in Fig. 7. The Fe 2p XPS profile of HMFeMoC0.1-800 (Fig. 7a) showed well distinguished peaks at the binding energies of 710.7 and 709.1 eV indicates the presence of iron in +3 and +2 oxidation states [39,40]. Based on the literature, the energy difference between the iron +2 and +3 levels should be for ~2 eV [40]. The present studies showed the difference in binding energy value of 1.6 eV was observed (710.7 - 709.1 = 1.6 eV) (Fe 2p3/2), the deviation may be due to the Fe-O-Mo species interaction. The Mo 3d core-level XPS profile of HMFeMoC0.1-800 (Fig. 7b) exhibited a Mo $3d_{5/2}$ peak at the binding energies of 231.1 and 231.7 eV, which was characteristic of the molybdenum present in the higher valent ($Mo^{5+/6+}$) oxidation state [41–44]. The XPS results indicates the formation of solid solution of metal oxides of magnesium-iron-molybdate was obtained after calcination, which was in good agreement with the aforementioned FT-IR data. The surface chemical composition of HMFeMoC0.1 sample was found to be 4 wt. % of molybdenum, 24.4 wt. % of iron and 7 wt. % of magnesium respectively and support the presence of surface exposed molybdenum and iron species and can be potential for catalytic activities.

3.2. Catalytic activity

The catalytic activity of HMFeMo catalysts was analyzed for the liquid-phase epoxidation of cyclooctene and oxidation of isoeugenol to vanillin, and the results are summarized in Sections 3.2.1 and 3.2.2, respectively.

3.2.1. Cyclooctene epoxidation

3.2.1.1. Catalyst screening. The catalytic activities of all the as-synthesized and 800 °C calcined catalysts were evaluated for cyclooctene epoxidation, and the results are presented in Fig. 8. All catalysts selectively yielded cyclooctene epoxide as the product. The cyclooctene yield of the pure HMFe sample was approximately 45%. The HMFeMo samples presented good cyclooctene epoxidation activity. Moreover, as the molybdate loading of the HMFeMo samples increased, the epoxide yields also increased. The HMFeMo0.1 sample presented the highest

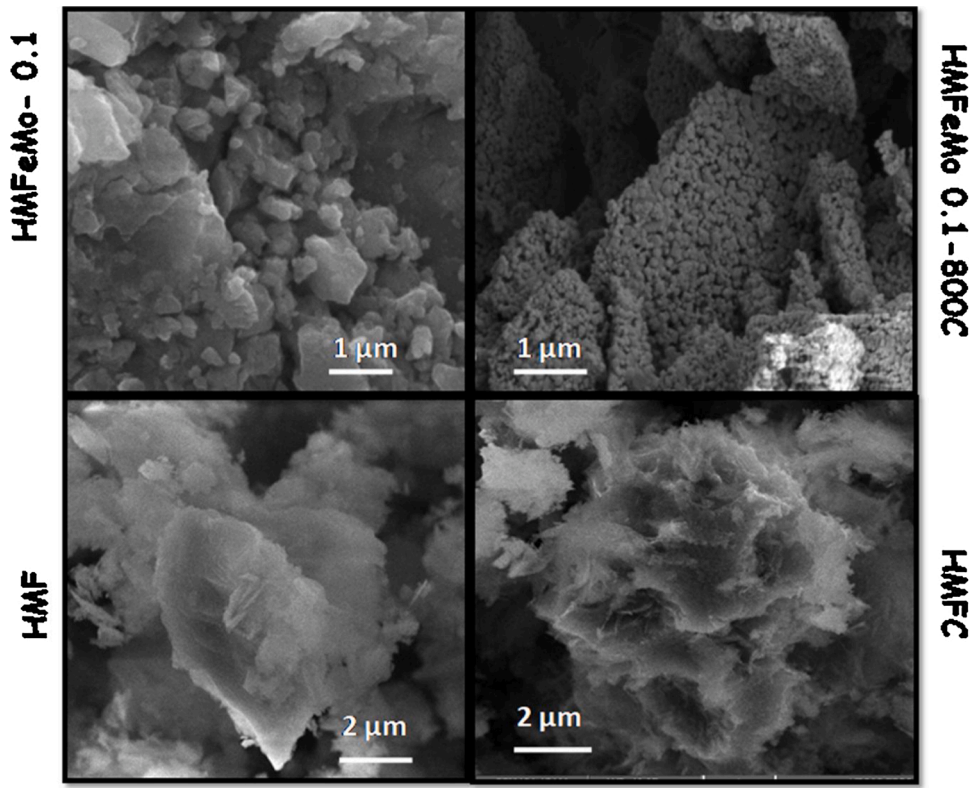

Fig. 4. Scanning electron microscopy images of as-prepared (a) HMFeMo0.1 and (b) HMFe and calcined (c) HMFeMoC0.1-800 and (d) HMFeC-800.

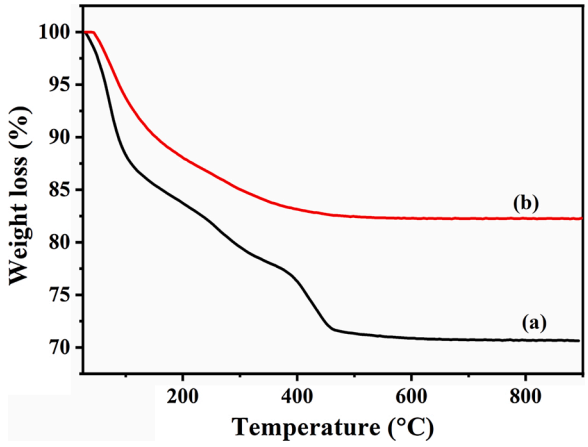

Fig. 5. Thermo-gravimetric analysis profiles of (a) HMFe and (b) HMFeMo0.1.

cyclooctene epoxide yield (86%) among all HMFeMo samples. Further increasing the molybdenum loading (HMFeMo0.15) led to a slight decrease in cyclooctene conversion (80%). The corresponding calcined samples followed the same trend for cyclooctene epoxidation, and the cyclooctene epoxide yield of HMFeMoC0.1-800 was 94%. These results suggested that HMFeMo0.1 was the most active catalyst for cyclooctene epoxidation among all as-prepared and calcined catalysts in this study may be due to uniform distribution of molybdenum species on the interlayer surface. Therefore, all subsequent experiments were performed using the HMFeMoC0.1-800 catalyst. The HMFe catalysts with Mg-O-Fe site shows comparable activity towards epoxidation reaction. The introduction of molybdenum results the presence of surface Mo-O-Fe-O species, which is the active site for the oxidation reactions [45]. Thus, the presence of surface exposed iron and molybdenum oxo species and synergistic effect of magnesium–iron can account for the observed activity in the cyclooctene epoxidation. Whereas upon higher molybdenum loading, the polyoxoanions species [34] are formed and results in a slightly decreased yield of cyclooctene epoxide. The reaction without catalyst was also studied, and its conversion was found to be below 10%.

3.2.1.2. Effect of calcination temperature. The catalytic activity of the HMFeMo0.1 samples calcined at different temperatures were explored for cyclooctene epoxidation, and the results are presented in Fig. S3. The increase in calcination temperature facilitated the increase in cyclooctene epoxide yield. The highest cyclooctene epoxide yield was achieved over the HMFeMoC0.1-800 sample (94 %). A further increase in calcination temperature (HMFeMoC0.1-1000) led to a significant decrease in cyclooctene conversion (48%) may be due to sintering of active sites.

3.2.1.3. Effect of reaction temperature. The effect of reaction temperature on the epoxidation of cyclooctene is presented in Fig. 9. Cyclooctene epoxide yield increased with increasing reaction temperature. At a low temperature (50 °C), the cyclooctene conversion over HMFeMoC0.1-800 was only 20 %. The increase in reaction temperature cyclooctene conversion steadily increases and reached 94 % at 70 °C. A complete conversion of cyclooctene to cyclooctene epoxide was achieved at 70 °C after 24 h.

3.2.1.4. Catalyst recyclability testing. The stability of the HMFeMoC0.1-800 catalyst during the cyclooctene epoxidation reaction was evaluated (Fig. 10). The recyclability test was performed by separating the catalyst from the reaction mixture via centrifugation, followed by solvent (isopropyl alcohol) washing, and drying at 80 °C overnight before using the catalyst for the next cycle. The conversion of cyclooctene (more than 90 %) remained unchanged (within the error limit) after four consecutive reaction cycles, indicating the high stability of the catalyst under the reaction conditions. The observed better activity during the recycle studies may be due to presence of molybdenum as oxo-species, which is

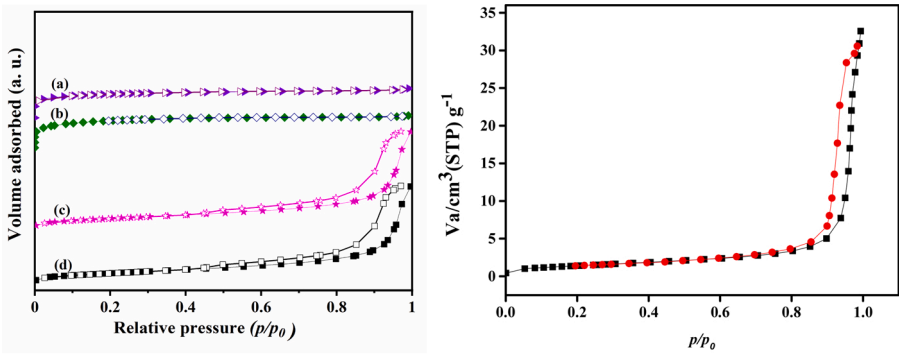

Fig. 6. Nitrogen adsorption–desorption isotherms of (1) (a) HMFeMo0.15, (b) HMFeMo0.1, (c) HMFeMo0.05, (d) HMFe and (2) HMFeMoC0.1-800.

Table 1
Textural properties of molybdate-intercalated magnesium-iron hydrotalcite materials.

Sl. no.	Sample	BET (m^2/g)	Pore volume (cm^3/g)
1	HMFe	77	0.26
2	HMFeMo0.05	77	0.26
3	HMFeMo0.1	182	0.09
4	HMFeMo0.15	177	0.08
5	HMFeMoC0.1-800 °C	5	0.04

formed in the presence of peroxide.

3.2.2. *Isoeugenol oxidation to vanillin*

The as-prepared and calcined HMFeMo and pure HMFe samples were further used for liquid-phase oxidation of isoeugenol to vanillin, and the results are summarized herein. The formation of vanillin from isoeugenol involves the oxidative cleavage of C = C to C–C bonds, followed by the formation of an aldehyde functionality. The anti-Markovnikov oxidation product, guaiacyl acetone and isomerised product eugenol, were formed as a side product (Scheme 1). In the presence of HMFeMo catalysts, isoeugenol oxidation yielded vanillin as the major product and guaiacyl acetone and eugenol as the minor products. The reaction did not proceed in the absence of a catalyst, and the formation of sticky products in the reactor was attributed to the formation of isoeugenol dimers and trimers.

3.2.2.1. Effect of molybdenum loading. HMFeMo samples with different molybdenum loadings were evaluated for isoeugenol oxidation, and the results are illustrated in Fig. 11. The isoeugenol conversion and selectivity toward vanillin of pure HMFe were 66 % and 72 %, respectively. As the molybdenum loading of HMFeMo increased, the isoeugenol conversion and selectivity toward vanillin also increased steadily. The presence of surface-exposed molybdenum oxo species and synergistic effect of magnesium–iron can account for the observed activity. The isoeugenol conversion and selectivity toward vanillin of HMFeMo0.1 were 86% and 83%, respectively. Upon further increasing molybdenum loading (HMFeMo0.15), a similar conversion was obtained; however, selectivity toward vanillin was lower (66%). A higher molybdenum loading can decrease material basicity [46], which can lead to a decrease in selectivity toward vanillin. When the isoeugenol oxidation reaction was performed using acetonitrile as the solvent, isoeugenol conversion was even lower (35%). This may be due to solvation of active species.

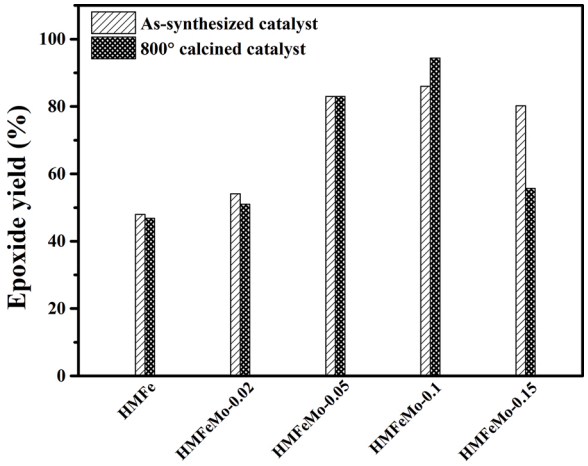

Fig. 8. Catalytic activity of the as-synthesized HMFeMo samples for cyclooctene epoxidation.

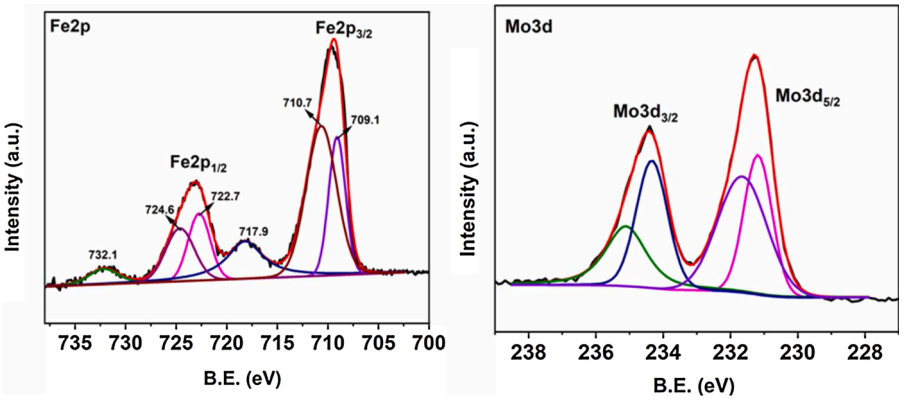

Fig. 7. (a) Fe 2p and (b) Mo 3d X-ray photoelectron spectroscopy profiles of HMFeMoC0.1-800.

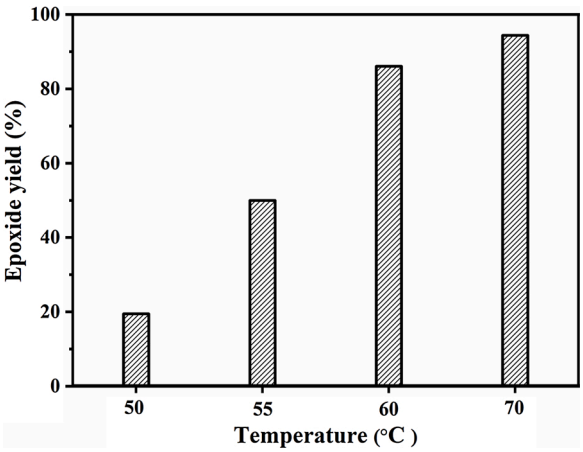

Fig. 9. Effect of reaction temperature on cyclooctene epoxidation over HMFeMoC0.1-800.

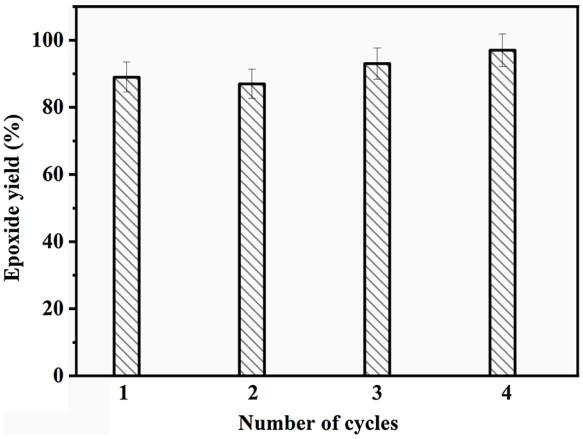

Fig. 10. Recyclability of HMFeMoC0.1-800 for cyclooctene epoxidation.

Therefore, all subsequent experiments were performed in the absence of solvents.

3.2.2.2. Effect of stirring rate. In order to understand the role of agitation on isoeugenol oxidation reaction, the conversion of isoeugenol and selectivity of vanillin was followed at different stirring rate. The reaction was studied at 200 rpm, 300 rpm, 500 rpm and 600 rpm and the conversion of *iso*-eugenol and vanillin selectivity was followed. The results are represented in Fig. 12. It is clear from the figure that the conversion of isoeugenol was increase from 48 % at 200 rpm to 83 % at 300 rpm. At lower stirring speed (200 rpm), under solid-liquid mass transfer limitations, the reaction is under diffusion control [47]. The conversion of isoeugenol and vanillin selectivity does not significantly change for agitation speed larger than 300 rpm and remain about 80 % might be due to better dispersion of reactant and oxidant on the surface and reaction becomes kinetic control [47].

3.2.2.3. Effect of catalyst amount. The effect of the substrate-to-catalyst ratio on the isoeugenol oxidation reaction was evaluated using the HMFeMo0.1 sample by varying the catalyst amount in the range of 0.025 to 0.1 g using 2 mmol of isoeugenol and 4 mmol of TBHP in decane as the reactant and oxidant, respectively, and the results are summarized in Fig. 13. When a small amount of catalyst (0.025 g) was used, the isoeugenol conversion and selectivity toward vanillin were 70% and 63%, respectively. Upon increasing the catalyst amount from 0.025 to 0.050 g, the isoeugenol conversion and selectivity toward vanillin increased and achieved a maximum. As the catalyst amount was further increased from 0.050 to 0.1 g the isoeugenol conversion and selectivity toward vanillin decreased to 67% and 64%, respectively. The use of excess catalyst results in polymerization of iso-eugenol and yield sticky-mass. The polymeric-sticky by-product formed using excess catalyst, deposit on the active surface and cause a decrease in the catalytic activity. This also yielded in low vanillin selectivity; thus, all subsequent experiments were performed using 0.05 g of catalyst.

3.2.2.4. Effects of different oxidants. The effects of different oxidants, namely TBHP in decane, TBHP in water (70%), cumene hydroperoxide, and H_2O_2 in water (30%) on the oxidation of isoeugenol to vanillin were studied (Fig. 14). The isoeugenol conversion and selectivity toward vanillin were 28% and 42.5% when TBHP in water (70%) was used as the oxidant. The isoeugenol conversion when H_2O_2 in water (30%) was used as the oxidant was only 18.5%. The isoeugenol conversion and selectivity toward vanillin were higher (62.9% and 56.3%, respectively) when cumene hydroperoxide was used as the oxidant. The highest isoeugenol conversion and selectivity toward vanillin (86% and 83%, respectively) were achieved when TBHP in decane was used as the oxidant. The use of aqueous peroxide, the water competitively adsorbed on the active surface and leads to poor activity. The use of organic oxidants and non-polar solvents (TBHP in decane) facilitate to bring efficiently the substrate and oxidant on the active surface and enhance the activity.

3.2.2.5. Effect of substrate-to-oxidant ratio. The effect of substrate-to-oxidant ratio (1:1, 1:2, 1:3, and 1:4) on the oxidation of isoeugenol to vanillin was analyzed, and the results are presented in Fig. 15. At a

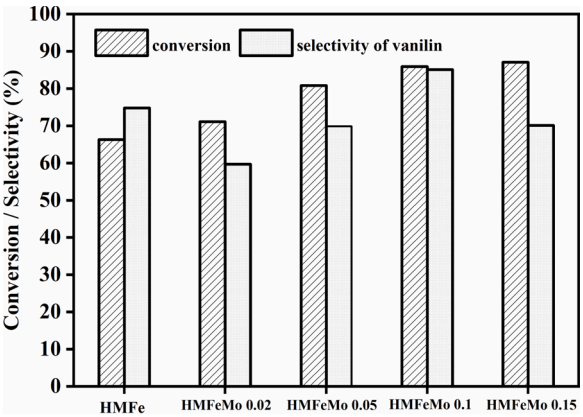

Fig. 11. Catalytic activity of the as-synthesized HMFeMo samples for isoeugenol oxidation.

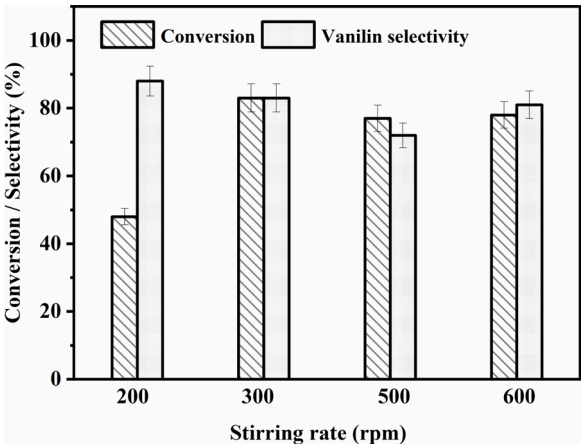

Fig. 12. Effect of stirring rate on isoeugenol oxidation.

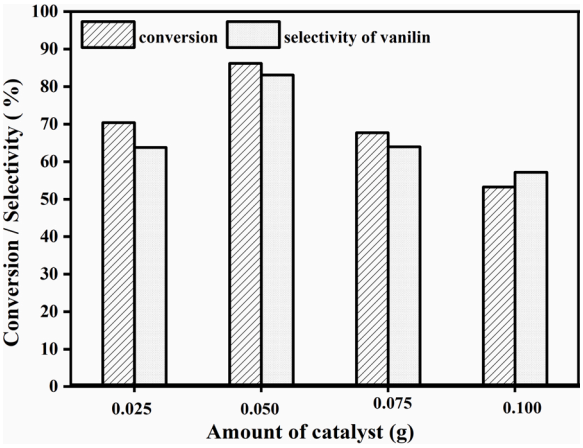

Fig. 13. The role of catalyst amount on isoeugenol oxidation.

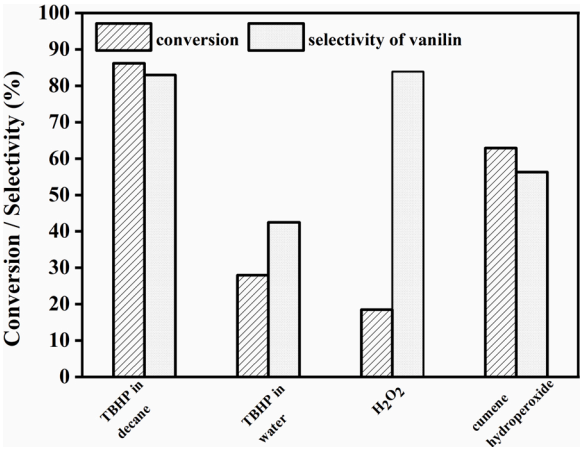

Fig. 14. Effect of several oxidants on isoeugenol oxidation.

substrate-to-oxidant ratio of 1:1, the isoeugenol conversion (63.6%) and selectivity toward vanillin (68.2%) were comparatively low. An isoeugenol conversion of 86% and a selectivity toward vanillin of 83% were achieved at a substrate-to-oxidant ratio of 1:2. Further increasing the amount of oxidant did not improve the isoeugenol conversion significantly. Therefore, the substrate-to-oxidant ratio for all subsequent experiments was selected to be 1:2.

3.2.2.6. Effect of temperature and time. The effect of reaction temperature on the isoeugenol oxidation reaction was evaluated at different temperatures for 90 min and the results are illustrated in Fig. S4. The isoeugenol conversion and selectivity toward vanillin increased steadily with increasing reaction temperature. At a high temperature of 110 °C, the isoeugenol conversion and selectivity toward vanillin were found to be 84 % and 83 %, respectively. A further increase in reaction temperature (at 120℃) resulted in the formation of a sticky bulky mass [48] owing to the oxidative polymerization of isoeugenol, which strongly bonded to the reactor walls, hindering product separation. Similarly, when the reaction was carried out for long duration at 100-110 ℃ considerable polymerization occurs. To improve the activity of the catalyst at lower temperature, we have chosen 80℃ as the reaction temperature and the reaction was followed at different duration. The results are displayed in Fig. S5. When the reaction time around 1.5 hr, the isoeugenol conversion was 63 % with vanillin selectivity of 81%. As the reaction time increases the steady improvement in the isoeugenol conversion observed and reaches maximum of 86% and vanillin selectivity of 83% is achieved at 5 hr. To the best of our knowledge the catalyst chosen in the present study (HMFeMo0.1) showed maximum vanillin selectivity (83 %) compared to other literature reported catalysts such as zeolite and cobalt based catalysts [24–26].

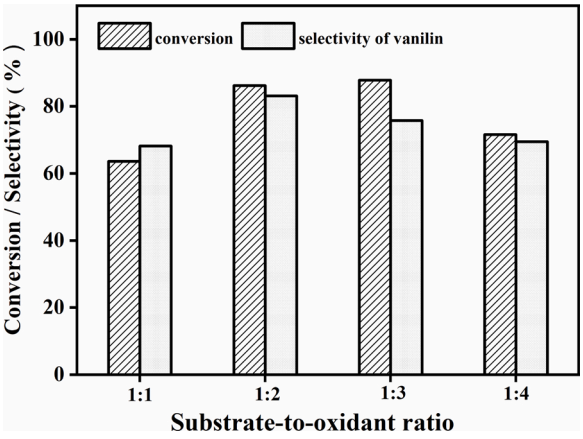

Fig. 15. Effect of substrate-to-oxidant ratio on isoeugenol oxidation.

3.2.2.7. Effect of calcination temperature. The HMFeMo0.1 catalyst was the most active catalyst under optimized reaction conditions. Furthermore, the effect of calcination temperature of the HMFeMo0.1 catalyst was studied for the selected catalytic reaction. The results (Fig. 16) indicated that as the catalyst calcination temperature increased, the isoeugenol conversion and selectivity toward vanillin decreased considerably. The increase in calcination temperature resulted in the collapse of the layered structure of the catalyst and the formation of Fe_2O_3 and Mo_2O_5, as confirmed by the FT-IR and XRD data, which can account for the observed decrease in isoeugenol conversion.

3.2.2.8. Recyclability study. Reusability is the most important property of heterogeneous catalysts. The recyclability of HMFeMo0.1 for isoeugenol oxidation under optimal reaction conditions was evaluated over four reaction cycles. The catalyst recovered after each cycle was washed with acetonitrile, dried, and calcined at 400 °C for 4 h to remove all adsorbed organic molecules before the next use. The isoeugenol conversion slightly decreased after the first run, whereas the selectivity toward vanillin remained almost unchanged for all reaction cycles (Fig. 17). Overall, the present catalyst HMFeMo0.1 catalyst showed maximum isoeugenol conversion of 86 % with the excellent vanillin selectivity of 83 % achieved under optimum conditions with comparable recyclability.

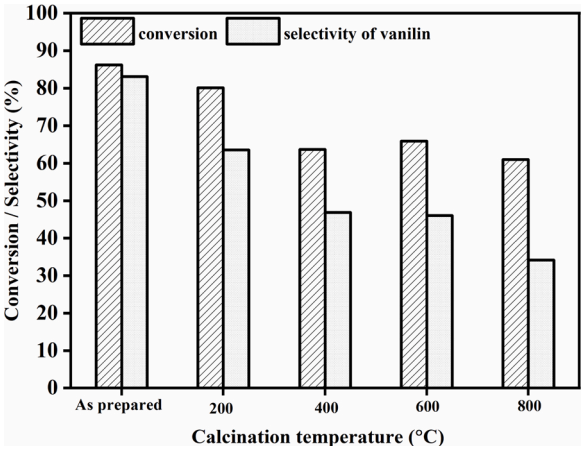

Fig. 16. Effect of calcinations temperature on isoeugenol oxidation over HMFeMo0.1.

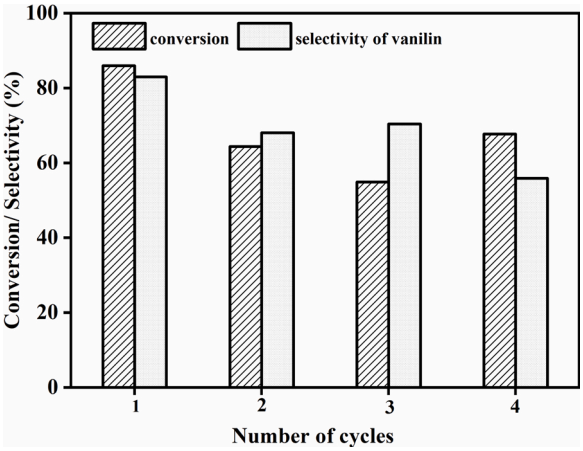

Fig. 17. Recyclability of HMFeMo0.1 catalyst for isoeugenol oxidation.

4. Conclusion

In this study, we developed a simple method for the preparation of molybdate intercalated magnesium-iron hydrotalcite (HMFeMo) materials. Powder XRD analyses revealed that the materials presented a layered HT structure and molybdate successfully intercalated and stabilized the layered iron based HT structure. TGA data indicated that the HMFeMo materials were more stable than pure HMFe. The as-synthesized HMFeMo materials were evaluated as catalysts for isoeugenol oxidation. Among the various catalysts prepared with different molybdate concentration, HMFeMo0.1 presented superior activity, with an isoeugenol conversion and a selectivity toward vanillin of 86% and 83%, respectively. Furthermore, HMFeMo0.1 presented a high activity and selectivity for cyclooctene epoxidation under mild reaction conditions; the activity of HMFeMo0.1 remained constant over several hours.

CRediT authorship contribution statement

A. Sakthivel: Conceptualization, Formal analysis, Writing – review and editing, Funding acquisition, Supervision. **P.P. Neethu:** Methodology, Data curation, Software, Formal analysis, Writing the draft of the manuscript. **A. Sreenavya:** Synthesis and reaction methodology, preparation of materials and Formal analysis and draft editing.

Declaration of Competing Interest

The authors declare that they have no known competing financial interests or personal relationships that could have appeared to influence the work reported in this paper.

Acknowledgement

The author thanks DST-SERB-CRG(Project No: CRG/2019/004624) for financial support. Neethu and Sreenavya are grateful to CSIR (File No. 09/1108(0036)/2019-EMR-1) and CUKfor the fellowship and Lab facilities.

Appendix A. Supplementary data

Supplementary material related to this article can be found, in the online version, at doi:https://doi.org/10.1016/j.apcata.2021.118292.

References

[1] A. Sreenavya, A. Sahu, A. Sakthivel, Hydrogenation of Lignin-derived phenolic compound eugenol over ruthenium-containig nickel hydrotalcite-type materials, Ind. Eng. Chem. Res. 59 (2020) 11979–11990.
[2] A. Sreenavya, T. Baskaran, V. Ganesh, D. Sharma, N. Kulal, A. Sakthivel, Framework of ruthenium-containing nickel hydrotalcite-type material: preparation, characterisation, and its catalytic application, RSC Adv. 8 (2018) 25248–25257.
[3] S. Albertazzi, F. Basile, A. Vaccari, Catalytic Properties of Hydrotalcite-Type Anionic Clays, Interface Sci. Technol. 1 (2004) 496–546.
[4] T. Baskaran, R. Kumaravel, J. Christopher, A. Sakthivel, Silicate anion-stabilized layered magnesium–aluminium hydrotalcite, RSC Adv. 3 (2013) 16392–16398.
[5] A. Fürstner, Iron catalysis in organic synthesis: a critical assessment of what it takes to make this base metal a multitasking champion, ACS Cent. Sci. 2 (2016) 778–789.
[6] V.R. Choudhary, R. Jha, P.A. Choudhari, Highly active and reusable catalyst from Fe-Mg-hydrotalcite anionic clay for Friedel-Crafts type benzylation reactions, J. Chem. Sci. 117 (2005) 635–639.
[7] N. Tahir, Z. Abdelssadek, D. Halliche, S. Saadi, R. Chebout, O. Cherifi, K. Bachari, Mg-Fe-hydrotalcite as catalyst for the benzylation of benzene and other aromatics by benzyl chloride reactions, Surface and Interface Analysis: An International Journal devoted to the development and application of techniques for the analysis of surfaces, interfaces and thin films 40 (2008) 254–258.
[8] T. Kawabata, N. Fujisaki, T. Shishido, K. Nomura, T. Sano, K. Takehira, Improved Fe/Mg-Al hydrotalcite catalyst for Baeyer–Villiger oxidation of ketones with molecular oxygen and benzaldehyde, J Mol Catal A Chem. 253 (2006) 279–289.
[9] P.S. Kumbhar, J. Sanchez-Valente, J.M.M. Millet, F. Figueras, Mg–Fe hydrotalcite as a catalyst for the reduction of aromatic nitro compounds with hydrazine hydrate, J. Catal. 191 (2000) 467–473.
[10] A.E. Stamate, O.D. Pavel, R. Zavoianu, I.C. Marcu, Highlights on the Catalytic Properties of Polyoxometalate-Intercalated Layered Double Hydroxides: A Review, Catalysts. 10 (2020) 57.
[11] D. Carriazo, S. Lima, C. Martín, M. Pillinger, A. Valente, V. Rives, Metatungstate and tungstoniobate-containing LDHs: Preparation, characterisation and activity in epoxidation of cyclooctene, J. Phys. Chem. Solids. 68 (2007) 1872–1880.
[12] F. Malherbe, C. Depege, C. Forano, J. Besse, M. Atkins, B. Sharma, S. Wade, Alkoxylation reaction catalysed by layered double hydroxides, Appl. Clay Sci. 13 (1998) 451–466.
[13] P. Mitchell, S. Wass, Propane dehydrogenation over molybdenum hydrotalcite catalysts, Appl. Catal. 225 (2002) 153–165.
[14] R. Zăvoianu, A. Cruceanu, O.D. Pavel, E. Angelescu, A.P.S. Dias, R. Bîrjega, Mechanisms, Oxidation of tert-butanethiol with air using Mo-containing hydrotalcite-like compounds and their derived mixed oxides as catalysts, React. Kinet. Mech. Catal. 105 (2012) 145–162.
[15] N.T. Thao, N.D. Trung, D. Van Long, Activity of molybdate-intercalated layered double hydroxides in the oxidation of styrene with air, Catal. Lett. 146 (2016) 918–928.
[16] R.R. Schrock, A.H. Hoveyda, Molybdenum and tungsten imido alkylidene complexes as efficient olefin-metathesis catalysts, Angew. Chem. Int. 42 (2003) 4592–4633.
[17] A. Sakthivel, M. Abrantes, A.S. Chiang, F.E. Kühn, Grafting of η5-Cp (COOMe) MoCl (CO) 3 on the surface of mesoporous MCM-41 and MCM-48 materials, J. Organomet. Chem. 691 (2006) 1007–1011.
[18] B. Rahmanivahid, M. Pinilla-de Dios, M. Haghighi, R.J.M. Luque, Mechanochemical Synthesis of CuO/MgAl2O4 and MgFe2O4 Spinels for Vanillin Production from Isoeugenol and Vanillyl Alcohol, Molecules 24 (2019) 2597.
[19] B.G. Harvey, A.J. Guenthner, H.A. Meylemans, S.R. Haines, K.R. Lamison, T. J. Groshens, L.R. Cambrea, M.C. Davis, W.W. Lai, Renewable thermosetting resins and thermoplastics from vanillin, Green Chem. 17 (2015) 1249–1258.
[20] M. Fache, B. Boutevin, S. Caillol, Vanillin production from lignin and its use as a renewable chemical, ACS Sustain. Chem. Eng. 4 (2016) 35–46.
[21] A. Bohre, D. Gupta, M.I. Alam, R.K. Sharma, B. Saha, Aerobic Oxidation of Isoeugenol to Vanillin with Copper Oxide Doped Reduced Graphene Oxide, Chemistry Select. 2 (2017) 3129–3136.
[22] A. Franco, S. De, A.M. Balu, A.A. Romero, R. Luque, Selective oxidation of isoeugenol to vanillin over mechanochemically synthesized aluminosilicate supported transition metal catalysts, Chemistry Select. 2 (2017) 9546–9551.
[23] E.V. Gusevskaya, L. Menini, L.A. Parreira, R.A. Mesquita, Y.N. Kozlov, G. B. Shul'pin, Oxidation of isoeugenol to vanillin by the "H2O2–vanadate–pyrazine-2-carboxylic acid" reagent, Mol. Catal. 363 (2012) 140–147.
[24] H. Mao, L. Wang, F. Zhao, J. Wu, H. Huo, J. Yu, Cobalt-catalyzed Aerobic Oxidation of Eugenol to Vanillin and Vanillic Acid, J Chin Chem Soc. 63 (2016) 261–266.
[25] I.B. Adilina, T. Hara, N. Ichikuni, S. Shimazu, Oxidative cleavage of isoeugenol to vanillin under molecular oxygen catalysed by cobalt porphyrin intercalated into lithium taeniolite clay, J. Mol. Catal. 361 (2012) 72–79.
[26] P. Sahu, V. Ganesh, A. Sakthivel, Oxidation of a lignin-derived-model compound: Iso-eugenol to vanillin over cerium containing MCM-22, Catal. Commun. 145 (2020) 106099, https://doi.org/10.1016/j.catcom.2020.106099.
[27] S. Paikaray, M.J. Hendry, In situ incorporation of arsenic, molybdenum, and selenium during precipitation of hydrotalcite-like layered double hydroxides, Appl. Clay Sci. 77 (2013) 33–39.
[28] M.J. Hernandez-Moreno, M.A. Ulibarri, J. Rendon, C.J. Serna, IR characteristics of hydrotalcite-like compounds, Phys. Chem. Miner. 12 (1985) 34–38.
[29] L. Mei, L. Liao, Z. Wang, C. Xu, Interactions between phosphoric/tannic acid and different forms of FeOOH, Adv. Mater. Sci. Eng. 2015 (2015).
[30] N.A. Dhas, A. Gedanken, Characterization of sonochemically prepared unsupported and silica-supported nanostructured pentavalent molybdenum oxide, J. Phys. Chem. B. 101 (1997) 9495–9503.
[31] N.B.-H. Abdelkader, A. Bentouami, Z. Derriche, N. Bettahar, L.C. De Menorval, Synthesis and characterization of Mg–Fe layer double hydroxides and its

application on adsorption of Orange G from aqueous solution, Chem. Eng. J. 169 (2011) 231–238.
[32] M.S. Kumar, M. Schwidder, W. Grünert, A.J. Brückner, On the nature of different iron sites and their catalytic role in Fe-ZSM-5 DeNOx catalysts: new insights by a combined EPR and UV/VIS spectroscopic approach, J. Catal. 227 (2004) 384–397.
[33] S. Dapurkar, S. Badamali, P. Selvam, Nanosized metal oxides in the mesopores of MCM-41 and MCM-48 silicates, Catal. Today. 68 (2001) 63–68.
[34] H. Tian, I.E. Wachs, L.E. Briand, Comparison of UV and visible Raman spectroscopy of bulk metal molybdate and metal vanadate catalysts, J. Phys. Chem. B 109 (2005) 23491–23499.
[35] R.L. Frost, A.W. Musumeci, T. Bostrom, M.O. Adebajo, M.L. Weier, W. Martens, Thermal decomposition of hydrotalcite with chromate, molybdate or sulphate in the interlayer, Thermochim. Acta. 429 (2005) 179–187.
[36] M. Thommes, K. Kaneko, A.V. Neimark, J.P. Olivier, F. Rodriguez-Reinoso, J. Rouquerol, K.S. Sing, Physisorption of gases, with special reference to the evaluation of surface area and pore size distribution (IUPAC Technical Report), Pure Appl. Chem. 87 (2015) 1051–1069.
[37] A. Vaccari, Preparation and catalytic properties of cationic and anionic clays, Catal. Today. 41 (1998) 53–71.
[38] D. Carriazo, C. Domingo, C. Martin, V. Rives, Structural and texture evolution with temperature of layered double hydroxides intercalated with paramolybdate anions, Inorg. Chem. 45 (2006) 1243–1251.
[39] P. Li, E. Jiang, H.L. Bai, Fabrication of ultrathin epitaxial γ-Fe2O3 films by reactive sputtering, J. Phys. D: Appl. Phys. 44 (2011) 075003.
[40] J.-C. Wanga, J. Rena, H.-C. Yaoa, L. Zhanga, J.-S. Wanga, S.-Q. Zanga, L.-F. Hanb, Z.J. Lia, Synergistic photocatalysis of Cr (VI) reduction and 4-Chlorophenol degradation over hydroxylated-Fe2O3 under visible light irradiation, J. Hazard. Mater. 311 (2016) 11–19.
[41] C. Clayton, Y.C. Lu, Electrochemical and XPS evidence of the aqueous formation of Mo2O5, Surf. Interface Anal. 14 (1989) 66–70.
[42] P.A. Spevack, N. McIntyre, A Raman and XPS investigation of supported molybdenum oxide thin films. 1. Calcination and reduction studies, J. Phys. Chem. 97 (1993) 11020–11030.
[43] J. Baltrusaitis, B. Mendoza-Sanchez, V. Fernandez, R. Veenstra, N. Dukstiene, A. Roberts, N. Fairley, Generalized molybdenum oxide surface chemical state XPS determination via informed amorphous sample model, Appl. Surf. Sci. 326 (2015) 151–161.
[44] X. Deng, S.Y. Quek, M.M. Biener, J. Biener, D.H. Kang, R. Schalek, E. Kaxiras, C. M. Friend, Selective thermal reduction of single-layer MoO3 nanostructures on Au (1 1 1), Surf. Sci. 602 (2008) 1166–1174.
[45] J.P. Falkenhagen, C. Limberg, S. Demeshko, S. Horn, M. Haumann, B. Braun, S. Mebs, Iron–molybdenum-oxo complexes as initiators for olefin autoxidation with O_2, Dalton Trans. 43 (2014) 806–816.
[46] V. Rives, D. Carriazo, C. Martín, Heterogeneous Catalysis by Polyoxometalate-Intercalated Layered Double Hydroxides, in: A. Gil, S. Korili, R. Trujillano, M. Vicente (Eds.), Pillared Clays and Related Catalysts, Springer, New York, NY, 2010, https://doi.org/10.1007/978-1-4419-6670-4_12.
[47] R. Kaur, R. Machiraju, K.D.P. Nigam, Agitation Effects in a Gas-Liquid-Liquid Reactor System: Methyl Ethyl Ketazine Production, Int. J. Chem. Reactor Eng. 5 (2007) A27.
[48] Hunay Evliya, Aral. Olcay, Oxidative Polymerisation of Isoeugenol and Mild Oxidation of Synthetic Polymers with Alkaline Cupric Hydroxide, International Journal of the Biology, Chemistry, Physics and Technology of Woo 28 (4) (1974) 130–135.